The Meteoritical Society

Meteoritics & Planetary Science 49, Nr 11, 2104–2117 (2014)
doi: 10.1111/maps.12305

^{53}Mn-^{53}Cr dating of aqueously formed carbonates in the CM2 lithology of the Sutter's Mill carbonaceous chondrite

Christine E. JILLY[1*], Gary R. HUSS[1], Alexander N. KROT[1], Kazuhide NAGASHIMA[1], Qing-Zhu YIN[2], and Naoji SUGIURA[3]

[1]Hawai'i Institute of Geophysics and Planetology, University of Hawai'i at Mānoa, Honolulu, Hawai'i 96822, USA
[2]Department of Earth and Planetary Sciences, University of California, Davis, Davis, California 95616, USA
[3]Department of Earth and Planetary Science, Graduate School of Science, the University of Tokyo, 7-3-1 Hongo, Bunkyo-ku, Tokyo 113-0033, Japan
[*]Corresponding author. E-mail: cjilly@hawaii.edu

(Received 09 September 2013; revision accepted 25 March 2014)

Abstract–Radiometric dating of secondary minerals can be used to constrain the timing of aqueous alteration on meteoritic parent bodies. Dolomite is a well-documented secondary mineral in CM chondrites, and is thought to have formed by precipitation from an aqueous fluid on the CM parent body within several million years of accretion. The petrographic context of crosscutting dolomite veins indicates that aqueous alteration occurred in situ, rather than in the nebular setting. Here, we present ^{53}Mn-^{53}Cr systematics for dolomite grains in Sutter's Mill section SM51-1. The Mn-Cr isotope data show well-resolved excesses of ^{53}Cr correlated with ^{55}Mn/^{52}Cr ratio, which we interpret as evidence for the in situ decay of radioactive ^{53}Mn. After correcting for the relative sensitivities of Mn and Cr using a synthetic Mn- and Cr-bearing calcite standard, the data yield an isochron with slope corresponding to an initial ^{53}Mn/^{55}Mn ratio of $3.42 \pm 0.86 \times 10^{-6}$. The reported error includes systematic uncertainty from the relative sensitivity factor. When calculated relative to the U-corrected Pb-Pb absolute age of the D'Orbigny angrite, Sutter's Mill dolomites give a formation age between 4564.8 and 4562.2 Ma (2.4–5.0 Myr after the birth of the solar system). This age is contemporaneous with previously reported ages for secondary carbonates in CM and CI chondrites. Consistent carbonate precipitation ages between the carbonaceous chondrite groups suggest that aqueous alteration was a common process during the early stages of parent body formation, probably occurring via heating from internal ^{26}Al decay. The high-precision isochron for Sutter's Mill dolomite indicates that late-stage processing did not reach temperatures that were high enough to further disturb the Mn-Cr isochron.

INTRODUCTION

Sutter's Mill, a witnessed meteorite fall, landed in the foothills of Sierra Nevada in northern California on April 22, 2012. Since its fall, nearly 100 specimens have been retrieved from the area. Initial characterization demonstrated that the meteorite is a carbonaceous chondrite regolith breccia with affinities to the CM group. Different lithologies exhibit varying degrees of thermal metamorphism, with inferred temperatures ranging from 153 ± 27 °C to approximately 500 °C in some lithologies (Jenniskens et al. 2012). The CM-like clasts are heavily aqueously altered, composed almost entirely of secondary minerals. These clasts apparently have not been heated significantly. The CM classification is confirmed by multiple studies, including geochemistry of light elements such as carbon and nitrogen (Grady et al. 2013), bulk chemistry, and whole-rock O and Cr isotopes (Jenniskens et al. 2012), which plot along CM trends. However, Jenniskens et al. (2012), Garvie (2013), and Ziegler and Garvie (2013) have identified clasts of different meteorite classes,

possibly indicating that the Sutter's Mill parent body is a rubble-pile asteroid.

The ^{53}Mn-^{53}Cr radiochronometer is well suited for dating of materials formed within the first approximately 20 Myr of solar system formation (e.g., Lugmair and Shukolyukov 1998; Shukolyukov and Lugmair 2006). ^{53}Mn decays into ^{53}Cr via electron capture, with a half-life of 3.7 Myr. This half-life is sufficiently long to resolve ages for aqueous alteration, thought to range between 1 and 15 Myr after formation of calcium-aluminum-rich inclusions (CAIs), which are believed to be the earliest-formed solar system objects (Krot et al. 2006). Secondary carbonate minerals are suitable targets for Mn-Cr dating as they fractionate Mn and Cr upon precipitation from an aqueous fluid. Mn acts as a compatible element and partitions into the carbonate crystal structure, while Cr remains incompatible (Pingitore et al. 1988). Radioactive ^{53}Mn leaves an excess of ^{53}Cr in the carbonate mineral after decay, which can then be measured via secondary isotope mass spectrometry (SIMS). This method of Mn-Cr dating has been used to determine the ages of precipitation for secondary carbonates in a variety of carbonaceous chondrites (e.g., Endress et al. 1996; Hoppe et al. 2007; De Leuw et al. 2009; Petitat et al. 2011; Fujiya et al. 2012, 2013; Lee et al. 2012). However, the accuracy of many previous measurements has been called into question due to the lack of proper standards and poorly constrained Mn/Cr relative sensitivity factors for carbonate minerals (Sugiura et al. 2010).

In this study, we present the in situ Mn-Cr isotope systematics from five secondary dolomite ($CaMg[CO_3]_2$) grains in Sutter's Mill section SM51-1 to date the carbonate formation time. All Mn-Cr dating was performed by SIMS. We discuss the systematic effect that poorly constrained relative sensitivity factors have on Mn-Cr SIMS measurements. We compare our results with other Mn-Cr carbonate measurements in carbonaceous chondrites, and discuss implications for the formation mechanism of carbonates on the Sutter's Mill parent body.

SAMPLES AND ANALYTICAL METHODS

Sutter's Mill SM51-1

A polished, carbon-coated thin section of Sutter's Mill (SM51-1) from the UC Davis collection was used in this study, and in the previous work of Jenniskens et al. (2012). The sample was analyzed with backscattered-electron imaging on a JEOL JSM-5900LV scanning electron microscope (SEM) to confirm the mineralogy and petrography discussed in previous studies, and to locate suitable ion probe targets. The SEM was set to an accelerating voltage of 15 kV, and energy-dispersive X-ray spectroscopy (EDS) was used to identify minerals.

Sutter's Mill section SM51-1 contains two main lithologies, CM 2.0 and CM 2.1, both dominated by secondary minerals (Jenniskens et al. 2012). The lithologies are similar in composition, with the primary difference being a higher abundance of anhydrous silicate grains (olivine and pyroxene) in the CM 2.1 clast. Both lithologies contain complete chondrule pseudomorphs embedded in an iron-rich phyllosilicate matrix; Mg-rich phyllosilicates also often display thin (approximately 1 μm) Fe-rich rims. Magnetite occurs frequently in the matrix of both lithologies, mostly as subhedral grains of approximately 20 μm in diameter. Small (approximately 5 μm) Fe,Ni-sulfides occur in the matrix and are associated with carbonate minerals. Calcite and dolomite are common, both in the matrix and within altered chondrules, as 10–50 μm sized equant grains. Dolomite crystals tend to be anhedral with many cracks, while calcite grains are often rounded, and are frequently intergrown with the dolomite (Fig. 1). Furthermore, dolomite veins crosscut the fine-grained rims of multiple chondrule pseudomorphs, indicating that aqueous alteration occurred in situ (Jenniskens et al. 2012) (Fig. 2). Jenniskens et al. (2012) reported on the compositions of representative calcite and dolomite in Sutter's Mill section 51-1. The calcite composition is nearly pure $CaCO_3$, containing <1 mol% of trace Fe, Mg, Mn, and Si in the mineral. The dolomite compositions deviate from the Ca:Mg = 1:1 stoichiometry, all containing an excess of calcium relative to magnesium (Ca/Mg > 1) (Jenniskens et al. 2012). These values are consistent with the dolomite compositions in other CM chondrites, shown to have Ca excesses >2 mol% $CaCO_3$, and dissimilar to the composition of CI dolomites, which tend to contain an excess of magnesium relative to calcium (Ca/Mg < 1) (De Leuw et al. 2010). The high abundance of dolomite and the relative lack of tochilinite in both the 2.0 and 2.1 lithologies of Sutter's Mill (Garvie 2013) are consistent with their characterization as heavily altered CM material (Rubin et al. 2007). However, De Leuw et al. (2010) suggest that dolomites disappeared from the most aqueously altered CMs due to the lack of dolomites observed in MET 01070 (CM 2.0). This observation is inconsistent with the CM 2.0 SM51-1 clast that contains many dolomites, indicating a different alteration environment between MET 01070 and SM51. Dolomite and calcite grains for Mn-Cr analysis were identified by their characteristic EDS spectra. The grains chosen for this study were >15 μm in diameter with uniform compositions.

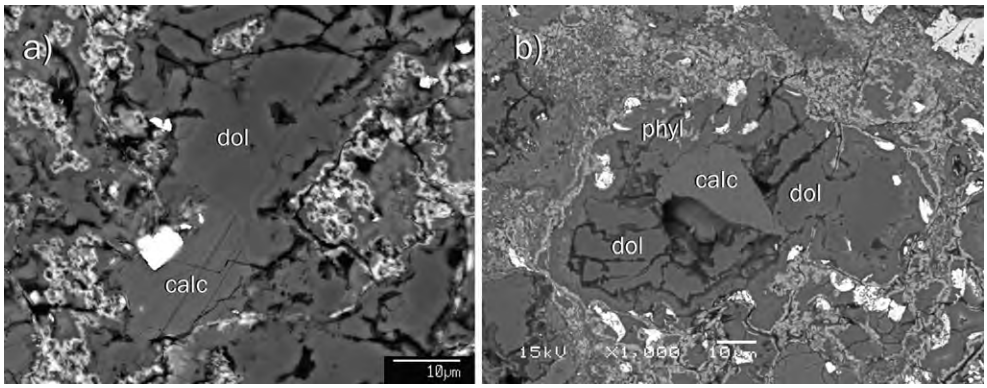

Fig. 1. BSE images of intergrown calcite and dolomite grains in SM 51-1.

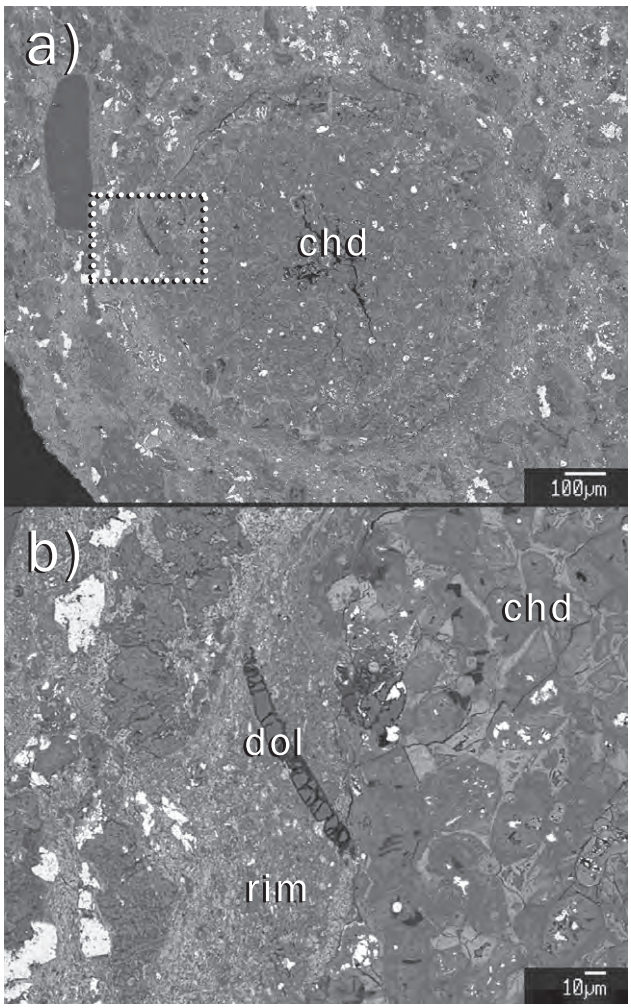

Fig. 2. a) Backscattered-electron image of a chondrule pseudomorph (chd) in SM 51-1, composed entirely of secondary minerals and phyllosilicates. The chondrule pseudomorph is surrounded by a fine-grained rim crosscut by dolomite veins, serving as evidence for in situ aqueous alteration on the CM parent body. The dotted square depicts the area of enlarged view (b) of a dolomite vein (dol) crosscutting the chondrule rim (rim).

Secondary Ion Mass Spectrometry

SIMS analysis was carried out using the University of Hawai'i Cameca ims-1280 ion microprobe. An $^{16}O^-$ primary beam with a total impact energy of 23 keV was used to sputter Mn and Cr isotopes from the sample. Masses $^{50}Cr^+$ (including interferences from $^{50}V^+$ and $^{50}Ti^+$), $^{52}Cr^+$, and $^{53}Cr^+$ were measured simultaneously in multicollection mode on electron multipliers (L2, C, and monocollection electron multipliers [EM]), followed by a peak jump to put $^{55}Mn^+$ on the monocollector EM. The mass resolving power for $^{50}Cr^+$ and $^{52}Cr^+$ was approximately 4400, and for $^{53}Cr^+$ and $^{55}Mn^+$ was approximately 6200, sufficient to resolve the interference from the $^{52}CrH^+$ ion on $^{53}Cr^+$. All samples and standards were presputtered for 600 seconds with a 300 pA beam and 5×5 μm^2 raster, followed by data collection at 100 pA with a beam spot size of 5 μm. Each spot analysis ran for approximately 100 cycles, with a total measurement time approximately 1.5 h. Automated centering of the secondary beam in the field aperture was applied before each measurement, and high-voltage offset control to compensate charging in the sputtered area was applied before and during each measurement. After the measurement, all ion probe pits were imaged to ensure that no cracks or impurities were included in the analysis.

All SIMS data were reduced using an in-house data reduction package. Isotope ratios were calculated from the summed total counts per run, rather than from the mean of the ratios in each cycle. The mean of the ratios method of calculating isotope ratios has been shown to introduce significant statistical bias, particularly for measurements with low count rates (Ogliore et al., 2011). The total counts method of calculating $^{55}Mn/^{52}Cr$ minimizes the risk of interpreting biased data as an isochron.

To correct for instrumental mass fractionation, two standards were measured during analysis: San Carlos

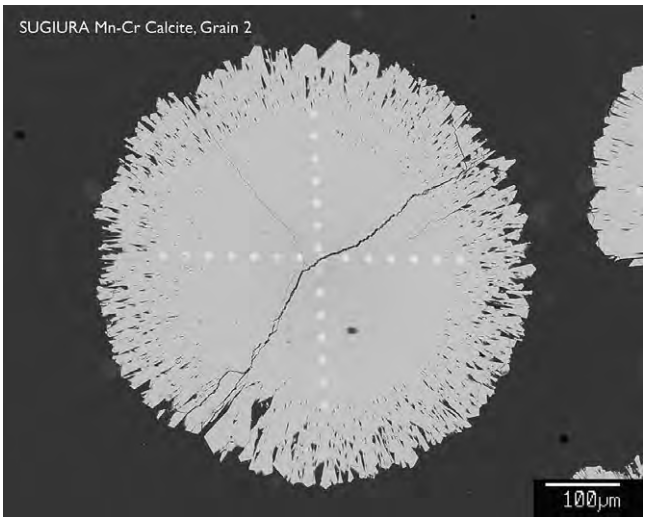

Fig. 3. Synthetic Mn- and Cr-bearing calcite crystal used for standardization. The light spots across the vertical and horizontal profiles are electron microprobe beam damage from characterization.

olivine, and synthetic Mn- and Cr-bearing carbonates. The compositions of the two standards were measured with electron microprobe analysis, discussed in the Relative Sensitivity Factors section below. Instrumental mass fractionation (IMF) was corrected for externally by comparing the mean $^{53}Cr^{+}/^{52}Cr^{+}$ ratio measured on the standards with the reference ratio, taken as $^{53}Cr/^{52}Cr = 0.113459 \pm 0.000005$ (Papanastassiou 1986). We could not do an internal mass fractionation correction because the interferences (^{50}V, ^{50}Ti) on ^{50}Cr were too large. Over the course of the measurements, the instrument was retuned once, which can alter the IMF; therefore, two separate IMF corrections have been applied to measurements from before and after retuning. ^{53}Cr excesses in the unknowns are reported as $\delta^{53}Cr^{*}$, representing the deviation of the IMF-corrected measurement ratios from the reference ratio in per mil (‰).

Relative Sensitivity Factors

The fractionation of Mn and Cr in carbonates makes them difficult to standardize for Mn-Cr radiometric dating. An optimum standard should be a homogeneous crystal of the same carbonate mineral as the unknown, containing measurable amounts of both Mn and Cr. Mn- and Cr-bearing carbonates do not occur commonly on Earth, and present a challenge to synthesize because Cr does not readily partition into the crystal structure. However, researchers at the University of Tokyo have recently successfully synthesized Mn and Cr-bearing calcite grains (Sugiura et al. 2010). We use some of these grains as a standard for carbonate Mn-Cr mass spectrometry in this study (Fig. 3).

The relative sensitivity factor (RSF)—defined here as $([^{55}Mn^{+}/^{52}Cr^{+}]_{SIMS}/[^{55}Mn/^{52}Cr]_{TRUE})$—represents the isotopic ratio measured by SIMS relative to the true isotopic ratio of the sample (however, the inverse is sometimes used in literature). The RSF is dependent on a number of factors, the most important being the mineral composition and instrument tuning (McKibbin et al. 2013). Historically, the RSF for silicate minerals or glasses has been used as a proxy for carbonate RSF (e.g., Hoppe et al. 2007; De Leuw et al. 2009; Petitat et al. 2011; Lee et al. 2012). However, recent studies have shown that the carbonate RSF differs significantly from that of olivine (Sugiura et al. 2010), therefore invalidating previously measured Mn-Cr carbonate isochrons. In this study, we have measured Mn and Cr isotopes in both San Carlos olivine and the synthesized Mn- and Cr-bearing calcites to compare the effect of RSF on carbonate isochrons. It should be noted that the difference in RSF for calcite and dolomite is currently unknown. For the purpose of this study, we will construct our isochrons based on the assumption that the RSFs for calcite and dolomite are indistinguishable. If the dolomite RSF is later found to differ from that of calcite, the data reported here should be corrected to the proper dolomite RSF.

To determine the value of $(^{55}Mn/^{52}Cr)_{TRUE}$ for both standards, elemental abundances were measured using the JEOL JXA-8500F electron microprobe at the University of Hawai'i. Because the synthetic-calcite crystals are zoned in Mn and Cr, each synthetic-calcite was characterized by two line profiles across the grain diameters, with measurements taken every 30 μm. For the synthetic carbonates, Ca, Si, Mg, Mn, and Cr were measured at 15 keV accelerating voltage for 30 seconds each. The beam current was set to a low 10 nA current, and a broad beam of 10 μm was used to minimize damage to the calcite grains. Detection limits (in elemental weight percent) were 0.019, 0.013, 0.013, 0.041, and 0.027 for Ca, Si, Mg, Mn, and Cr, respectively. Carbonate measurements were standardized to rhodochrosite, chromite USNM 117075, San Carlos Olivine USNM 111312, and calcite standards. The carbon content was calculated stoichiometrically relative to cations by assuming that there are 0.333 atoms of C per 1 atom of O. SIMS spot analyses for the calcite standards were then taken directly on the measured electron probe spots to avoid the small-scale heterogeneity and zoning. For San Carlos olivine, electron microprobe analysis was conducted after the SIMS data collection. Seven points surrounding the ion

probe pits were measured for Si, Mg, Fe, Mn, Ni, Cr, Al, and Ca with count times ranging from 20 to 90 s. Beam parameters were optimized for detecting Mn and Cr in olivine at 20 keV and 50 nA. San Carlos olivine measurements were standardized to San Carlos olivine USNM 111312, Rockport MA fayalite USNM 85276, Verma garnet, and chromite USNM 117075. All EPMA data were routinely corrected using the ZAF method.

To calculate ^{52}Cr concentrations from the EPMA data, the atomic Cr abundance was multiplied by the isotopic abundance of ^{52}Cr (0.83789; Baum et al. 2002). No correction factor is needed for ^{55}Mn, as it is the only stable isotope of Mn. RSF values for each standard were then obtained by dividing the measured SIMS $^{55}Mn^+/^{52}Cr^+$ ratio with the $^{55}Mn/^{52}Cr$ EPMA ratio.

RESULTS

EPMA results are shown in Fig. 4, plotting the variation in elemental abundance across the standard grain profile. All abundances are shown in atomic percent rather than weight percent for ease of comparison to the RSF. The calcite grain shows radial zoning in both Mn and Cr, but variable $^{55}Mn/^{52}Cr$ ratios. Combined errors are depicted on the Mn/Cr ratios, propagated from the total counts of the peak minus background for each point. Interior points had more stable Mn/Cr ratios due to higher Mn and Cr abundances; therefore, SIMS standard measurements were preferentially taken around the center of the calcite crystal. Considering only the region between 90 and 300 μm in the calcite standard (Fig. 4), the average value of $^{55}Mn/^{52}Cr$ measured by EPMA is 1.32 ± 0.28 (2σ standard deviation). However, as each individual SIMS spot was measured directly by EPMA, we use the $^{55}Mn/^{52}Cr$ ratio measured for that spot, rather than the average value, to calculate the RSF. The time-averaged synthetic-calcite RSF was 0.71 ± 0.16 (2σ), compared to a higher RSF of 0.86 ± 0.06 in San Carlos olivine (Fig. 5); all Sutter's Mill data are corrected with the calcite RSF. Error bars in Fig. 5 represent the propagated errors from SIMS and EPMA data. The scatter in the RSF values for the synthetic calcite standard was found to exist regardless of whether EPMA measurements were taken before or after SIMS measurements.

Seven points in five Sutter's Mill dolomite grains were measured for Mn-Cr. All but one of the grains were in the petrologic type 2.0 clast; the last grain was in the type 2.1 lithology (see Fig. 6). The analyzed dolomite grains ranged from 20 to 50 μm in diameter, occurring in the phyllosilicate matrix either as isolated grains or within larger aggregates of carbonate minerals.

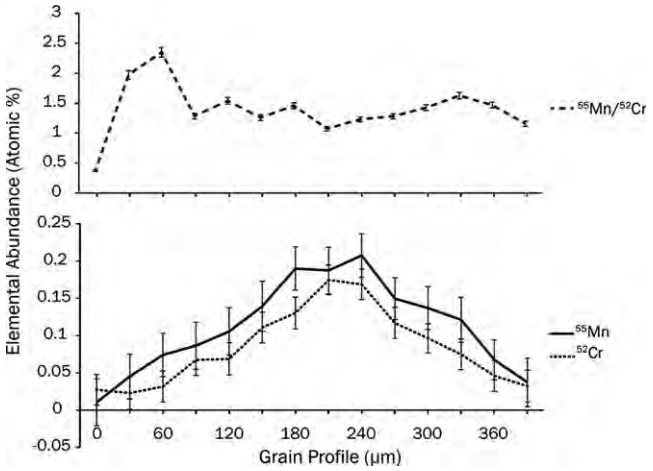

Fig. 4. Graph depicting the heterogeneity of manganese and chromium in the synthetic calcite standards. Please note the different scales on the y axes. Both manganese and chromium show radial zoning across the grain profile. However, the $^{55}Mn/^{52}Cr$ does not display a predictable trend toward the grain edges. Elemental abundances are given in atomic %, measured by the electron microprobe.

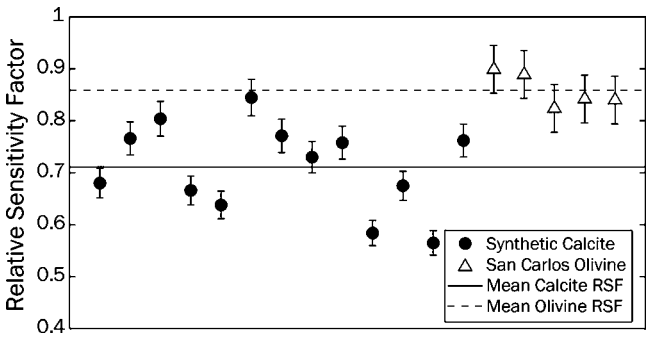

Fig. 5. The relative sensitivity factors (RSF) of each standard measurement for both San Carlos olivine and a synthetic Mn- and Cr-bearing calcite. The RSF is defined as $([^{55}Mn^+/^{52}Cr^+]_{SIMS}/[^{55}Mn/^{52}Cr]_{TRUE})$, where the solid line represents an average value for the calcite RSF of 0.71 ± 0.16, and the dotted line represents the average value of the San Carlos olivine RSF of 0.86 ± 0.06. However, we stress that the average RSF value for calcite is significantly less than for olivine.

Multiple calcite grains were targeted as well; however, due to mineral purity, the measurements yielded Mn and Cr count rates far too low for radiometric dating. Mn-Cr data from Sutter's Mill SM51-1 dolomites are listed in Table 1. $\delta^{53}Cr^*$ in dolomite ranges up to $1220.6 \pm 165.5‰$, and the $^{55}Mn/^{52}Cr$ ranges up to 38327 ± 1260 (after RSF correction). The errors reported are 2σ. For $^{55}Mn/^{52}Cr$ in Table 1, we report the 2σ internal error on the measurements not including the systematic uncertainty from the RSF.

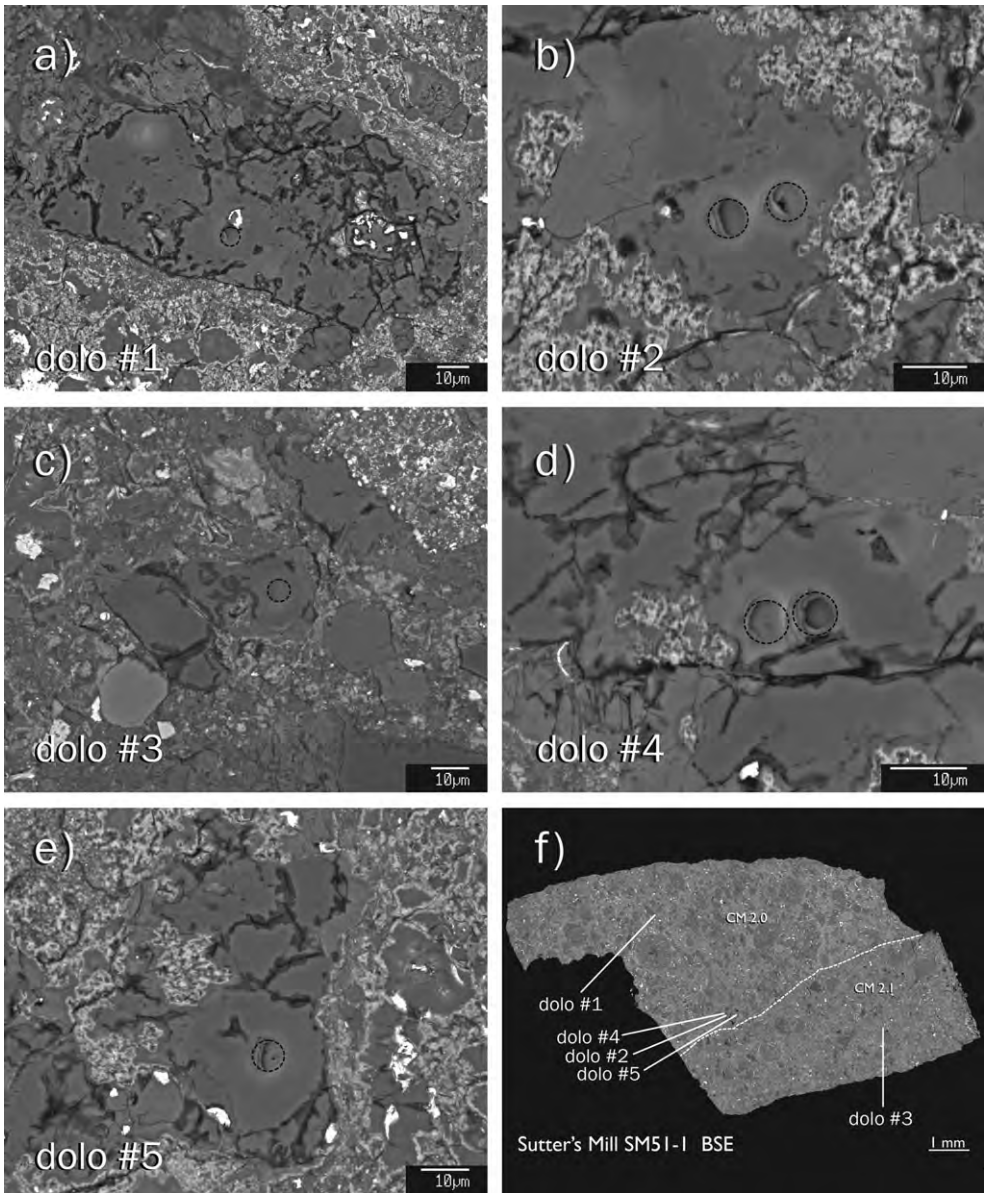

Fig. 6. a–e) Backscattered-electron images of the five SM51-1 dolomite grains measured for Mn-Cr. Ion probe spots are designated by the black dashed circles. f) Backscattered-electron image of the SM51-1 thin section, showing the CM 2.0/CM 2.1 clast boundary and dolomite grain locations.

Table 1. Mn-Cr isotope data from dolomite grains in Sutter's Mill SM 51-1.

Grain	$^{55}Mn/^{52}Cr$[a]	^{55}Mn total counts[b]	$^{53}Cr/^{52}Cr$[a]	$\delta^{53}Cr^{*}$[a]
dol #1	145.7 ± 0.4	67739	0.11494 ± 0.00088	13.0 ± 7.8
dol #2a	6620.5 ± 103.8	34213	0.13608 ± 0.00628	199.4 ± 55.3
dol #2b	38326.6 ± 1259.6	36134	0.25195 ± 0.01878	1220.6 ± 165.5
dol #3	3277.7 ± 62.3	11592	0.12489 ± 0.00720	100.8 ± 63.5
dol #4a	13864.4 ± 350.6	27534	0.15728 ± 0.01097	386.2 ± 96.6
dol #4b	2022.4 ± 19.8	33902	0.12203 ± 0.00363	75.6 ± 32.0
dol #5	8558.8 ± 154.3	33443	0.14366 ± 0.00739	273.8 ± 65.2

[a]Errors are 2σ, not including uncertainty in the RSF.
[b]Sum of all counts per run, normalized by number of cycles per run.

A diagram of $^{53}Cr/^{52}Cr$ versus $^{55}Mn/^{52}Cr$ is displayed in Fig. 7, showing clear evidence for excess ^{53}Cr correlated with $^{55}Mn/^{52}Cr$ ratio in the dolomites. The slope of the correlation trend corresponds to value of $3.42 \pm 0.36 \times 10^{-6}$ during the precipitation of dolomite. The error bars in Fig. 7 represent the 2σ statistical uncertainty in the measurements, not including the systematic uncertainty in the carbonate RSF. The low value of $\chi_{red}^2 = 0.28$ (also equal to MSWD) indicates either that the errors are overestimated, or that the stochastic fluctuations in the data have led to a good agreement between the data and the fitted isochron. One major contribution to the low χ_{red}^2 is the propagation of the IMF standard error into the uncertainty in $^{53}Cr/^{52}Cr$. Although we did not witness a nonstochastic fluctuation in our standard measurements, we chose to be conservative with errors. Without the IMF error, the χ_{red}^2 value would double. Furthermore, the data do not show a strong correlated error that can commonly lead to a low χ_{red}^2 value. Other errors calculated are not likely overestimated, as they are dominated by the square root of the total counts, and do not include the error to the RSF.

Figure 8 demonstrates the effect of variable RSF on the isotope data. Although we use a value of 0.71 for the RSF, the slope of the correlation may be steeper or shallower when the error of ±0.16 is taken into account. This error corresponds to a range of $(^{53}Mn/^{55}Mn)_0$ from 4.19×10^{-6} for an RSF of 0.87, to 2.65×10^{-6} for an RSF of 0.55. If we propagate the 2σ standard deviation from the RSF into the dolomite $^{53}Cr/^{52}Cr$ versus $^{55}Mn/^{52}Cr$ trend, the uncertainty on the slope increases to $3.42 \pm 0.86 \times 10^{-6}$.

To determine the absolute ages of formation, Mn-Cr data are anchored to the U-isotope–corrected Pb-Pb ages of the D'Orbigny angrite. D'Orbigny is a quenched angrite (e.g., Mittlefehldt et al. 2002; Kleine et al. 2012) with an initial $(^{53}Mn/^{55}Mn)_0$ ratio of $(3.24 \pm 0.04) \times 10^{-6}$ (Glavin et al. 2004) and absolute Pb-Pb age of 4563.37 ± 0.25 Ma (Amelin et al. 2010; Brennecka and Wadhwa 2012). By assuming homogeneous ^{53}Mn distribution in the chondrite-forming region of the early solar system (Trinquier et al. 2008), we can compare the relative initial $(^{53}Mn/^{55}Mn)_0$ ratio of Sutter's Mill with that of D'Orbigny, to obtain an absolute age of 4563.7 $^{+1.1}/_{-1.5}$ Ma for the Sutter's Mill dolomite grains. This corresponds to a formation age between 2.4 and 5.0 Myr after the formation of CV CAIs (CAI formation age of 4567.30 ± 0.16 Ma from Connelly et al. [2012]). Errors in the absolute age for the Sutter's Mill dolomites include the 2σ statistical uncertainty in measurement and the systematic uncertainty in the RSF, and the uncertainty in the Mn-Cr age of D'Orbigny.

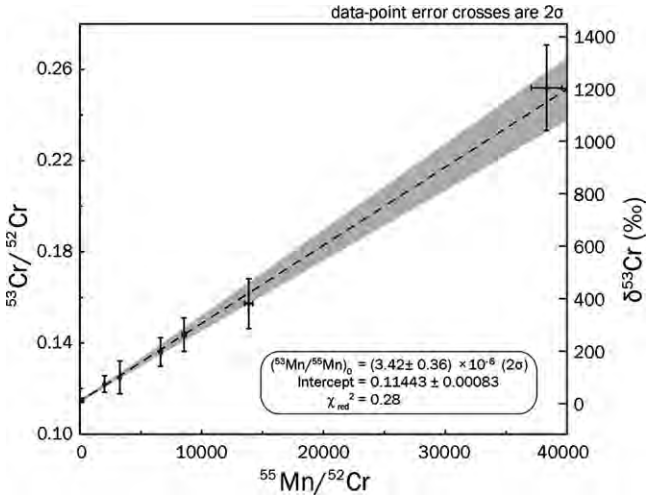

Fig. 7. $^{55}Mn/^{52}Cr$ versus $^{53}Cr/^{52}Cr$ diagram for dolomites in Sutter's Mill SM51-1, corrected to an RSF value of 0.71. $\delta^{53}Cr$ values are plotted on the right for reference. Error bars are 2σ internal error, not including systematic uncertainty in the RSF. Gray region indicates the 2σ error envelope.

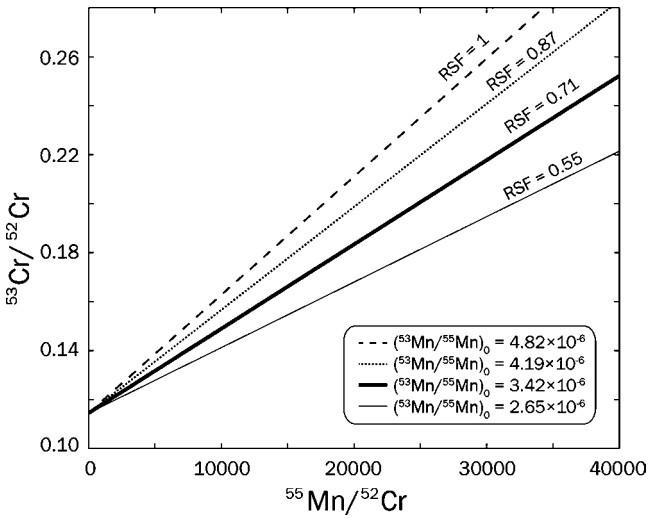

Fig. 8. The Sutter's Mill initial $(^{53}Mn/^{55}Mn)_0$ changes to a steeper or shallower slope depending on the value of the RSF used. In this study, we use an RSF for Mn-, Cr-bearing calcite of 0.71 ± 0.16 (2σ), as shown by the thick black line. Including the RSF uncertainty into the slope of the Mn-Cr correlation, we get $(^{53}Mn/^{55}Mn)_0 = 3.42 \pm 0.86 \times 10^{-6}$.

DISCUSSION

Aqueous Alteration in the CM Parent Body

The excesses of ^{53}Cr correlated with the Mn/Cr ratio in Sutter's Mill dolomites can, in principle, either

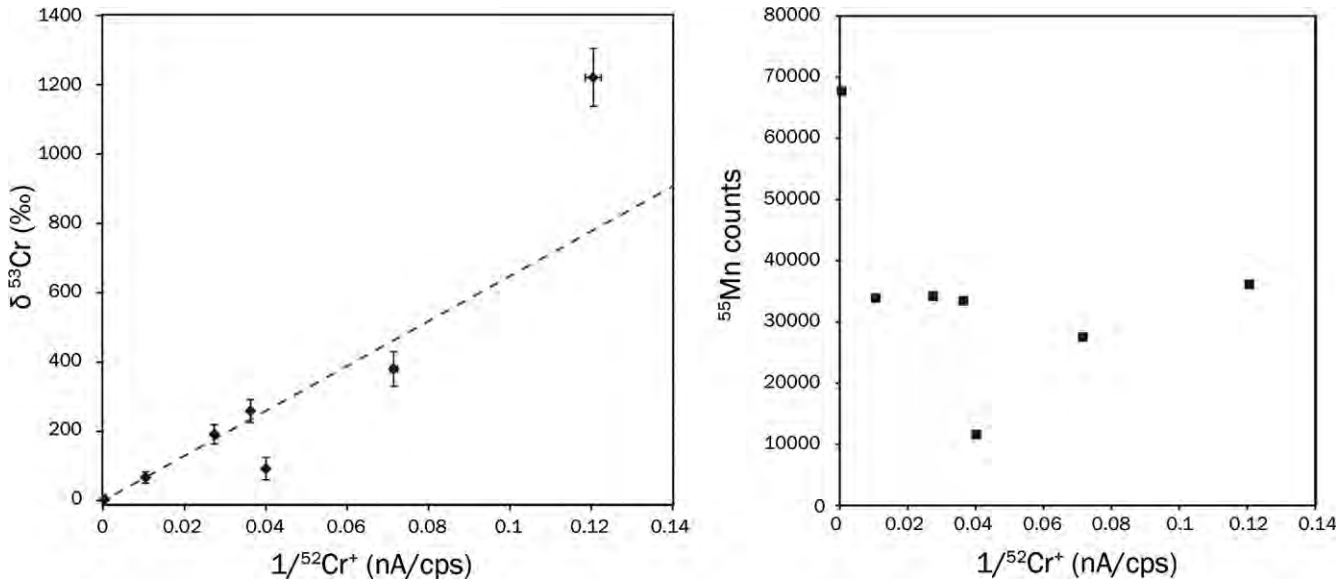

Fig. 9. Graphs of $\delta^{53}Cr$ versus $1/^{52}Cr^+$ and ^{55}Mn versus $1/^{52}Cr^+$. The $1/^{52}Cr^+$ values are given in counts per second, normalized to beam current. ^{55}Mn values are given as total counts, normalized to the number of cycles per run. The variability in $1/^{52}Cr^+$ and ^{55}Mn supports the interpretation of our data as an isochron.

be interpreted as an isochron, or as a mixing line of the carbonate mineral with a Cr-rich contaminant phase. The ^{55}Mn contents in each measurement can be used to distinguish whether this trend is an isochron or not (e.g., Hoppe et al. 2007); total counts of ^{55}Mn are presented in Table 1 and Fig. 9. The counts of ^{55}Mn vary from grain to grain, supporting a high time significance of our $\delta^{53}Cr$ and $^{55}Mn/^{52}Cr$ correlation. The Mn abundances in the dolomite grains are variable by a factor >2, suggesting that the observed correlation of $\delta^{53}Cr$ with $^{55}Mn/^{52}Cr$ probably represents zoning of Mn and Cr in the carbonate mineral during precipitation, rather than contamination from a Cr-bearing phase. Furthermore, plotting $\delta^{53}Cr$ versus $1/^{52}Cr^+$ yields a trend with a much larger MSWD of approximately 12 (Fig. 9). A mixing line would result in a better correlation than the isochron, which is not the case for our data. Therefore, we take the well-resolved excesses of ^{53}Cr to indicate the in situ decay of live ^{53}Mn at the time of carbonate precipitation.

We interpret the ^{53}Mn-^{53}Cr trend as an isochron, providing evidence for the early onset of aqueous alteration on the Sutter's Mill parent body. Petrographically, the Sutter's Mill section SM 51-1 shows compelling evidence for in situ alteration in the formation of the secondary dolomite. Dolomite veins that crosscut the rims of chondrule pseudomorphs are indicative of alteration on the parent body, rather than in the nebular setting (cf. Fig. 2). Hence, the aqueous alteration must have occurred after formation and accretion of the chondrules and matrix material. Possible sources of heating to drive aqueous alteration on the parent body include the internal decay of radioactive ^{26}Al, and impact heating. Our age is consistent with the idea that aqueous alteration was driven by heating from radioactive ^{26}Al in the Sutter's Mill parent body (e.g., Fujiya et al. 2012, 2013), soon after accretion. However, the impact-heating scenario cannot be entirely ruled out from this data set alone.

Many previous studies have used the ^{53}Mn-^{53}Cr system to constrain the timing and duration of aqueous alteration in carbonaceous chondrites (e.g., Endress et al. 1996; Hoppe et al. 2007; De Leuw et al. 2009; Petitat et al. 2011; Fujiya et al. 2012, 2013; Lee et al. 2012). To make accurate cross-laboratory comparisons with our results, there are two factors that must be addressed: absolute time anchors and relative sensitivity factors. Previous reports of absolute Pb-Pb ages assumed a constant $^{238}U/^{235}U$ composition for solar system materials. However, recent studies have shown that uranium isotopes may vary, and therefore must be measured to obtain correct Pb-Pb ages (Amelin et al. 2010; Brennecka and Wadhwa 2012). Brennecka and Wadhwa (2012) showed that angrite time anchors do contain deviations in U-isotopes, resulting in absolute age differences of >1 Myr from uncorrected measurements. The D'Orbigny angrite anchor used here has been extensively studied and corrected for such uranium-isotopic anomalies (Amelin 2008; Brennecka and Wadhwa 2012). D'Orbigny is a favorable time anchor as it yields consistent Mn-Cr, Pb-Pb, and Hf-W ages,

and well-behaved Al-Mg systematics (Glavin et al. 2004; Kleine et al. 2012). Furthermore, D'Orbigny is a quenched angrite, rather than plutonic (Keil 2012), which means that closure times for the different systems are likely to be concordant, even for the short-lived radiochronometers.

As discussed earlier, the RSF for carbonates can change the slope of an isochron, and therefore should be independently measured on a carbonate standard under the same conditions as the unknowns. Prior studies have used silicate mineral or glass standards (Endress et al. 1996; Hoppe et al. 2007; Petitat et al. 2011; Lee et al. 2012), or have used a previously determined RSF from literature to correct their data (e.g., De Leuw et al. 2009), introducing significant error into the results. However, the new RSF measurements for Mn- and Cr-bearing calcite grains have large uncertainties, as seen in Fig. 5. The uncertainty in our measured RSF is much larger than that for the electron probe data (Fig. 4), suggesting that there are small-scale heterogeneities in the calcite standards. While these standards are not perfect, they currently provide the best estimate of the true carbonate RSF.

We should be able to compare our Mn-Cr age in Sutter's Mill dolomite grains with ages obtained for other carbonaceous chondrite carbonates from the studies of Fujiya et al. (2012, 2013), as their measurements use the same synthetic calcite standards as in this study, with similar values determined independently for the RSF. Figure 10 shows the age range for Sutter's Mill carbonates compared with the in situ Mn-Cr ages for carbonates in other CM and CI chondrites of varying petrologic type. Errors bars for the Sutter's Mill age include the systematic error in the RSF. All data in Fig. 10 are anchored to D'Orbigny angrite. Sutter's Mill dolomites give the largest $^{53}Mn/^{55}Mn$ value, corresponding to the oldest age. However, within uncertainties, the ages are contemporaneous. Furthermore, to obtain a rough idea of how previous silicate-normalized measurements compare with this study, we can correct the published $(^{53}Mn/^{55}Mn)_0$ from literature using the difference in San Carlos olivine and carbonate RSF obtained in this study (this value is similar to that found by Fujiya et al. 2012). Assuming that the relative difference in RSF between silicate and carbonate is more or less independent of the lab, the isochron slopes can be corrected by the factor: $RSF_{calcite}/RSF_{olivine} = 0.83$, and reanchored to D'Orbigny angrite. Carbonate data from the literature for CM and CI carbonates yield carbonate formation ages between 2.4 and 5.1 Myr after CAI formation, consistent with this study (Hoppe et al. 2007; De Leuw et al. 2009; Petitat et al., 2009, 2011; Lee et al. 2012). However, caution should be taken with

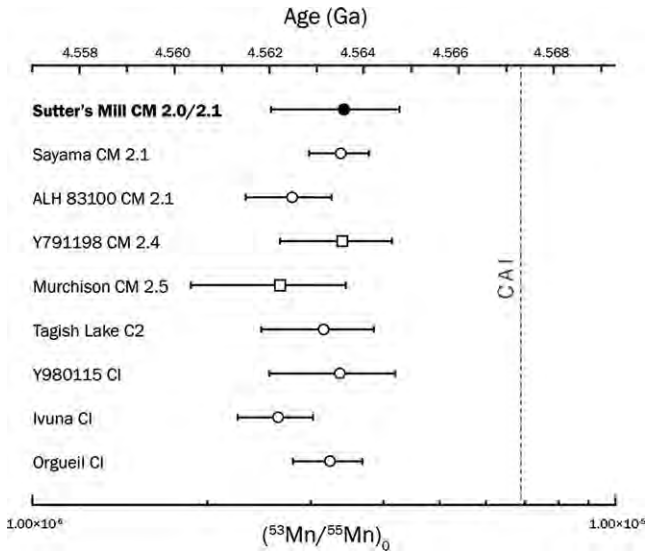

Fig. 10. Mn-Cr ages and initial $(^{53}Mn/^{55}Mn)_0$ for carbonates in carbonaceous chondrites. All Mn-Cr ages are anchored to D'Orbigny angrite U-corrected Pb-Pb data (Brennecka and Wadhwa 2012). The Sutter's Mill dolomite age from this study is indicated by a closed symbol. CI, CM, and Tagish lake data are indicated in open symbols, where the data are from Fujiya et al. (2012, 2013), recalculated to the D'Orbigny anchor. Dolomites are indicated as circles, calcites as squares. The Pb-Pb age for CV CAIs is shown as a dashed line (Connelly et al. 2012). The age for carbonate formation in Sutter's Mill SM51-1 is contemporaneous with carbonate formation in other carbonaceous chondrites.

these rough values as the magnitude of the RSF correction factor between San Carlos olivine (or other silicates) and carbonate is not necessarily the same for all instruments and studies.

The timing of carbonate formation in CM chondrites has been suggested to correlate with petrologic type (De Leuw et al. 2009). Their study measured the dolomite Mn-Cr ages in CM chondrites, and compared the results with previously measured carbonates in CI and CM chondrites, noting that the petrologic subtype correlates with carbonate age. De Leuw et al. (2009) conclude that alteration started contemporaneously throughout the CM parent body and that CM chondrites of lower petrologic subtype (more aqueously altered) experienced alteration over a longer period of time than CM chondrites of higher petrologic subtype (less aqueously altered). However, they did not independently measure the RSF for their instrumental setup, and compare literature data corrected to a variety of standards. In contrast to their results, our data, as well as data from Fujiya et al. (2012, 2013), do not show any observable correlation between the age of carbonates and the petrologic type. If such a correlation does exist, then the age differences

occurred on a short time scale that is currently unresolvable by the Mn-Cr chronometer. Another possible scenario is that the differences in petrologic type on the CM parent body reflect heterogeneous accretion of water-ice to the parent body, where lower petrologic type corresponds to a larger amount of ice incorporated into the rock.

Previous measurements of carbonates in CM chondrites have suggested that aqueous alteration on the asteroidal parent body may have occurred nearly contemporaneously with CAI formation (De Leuw et al. 2009; Tyra et al. 2009). However, as mentioned in De Leuw et al. (2009), these ages are anchored to the poorly constrained initial $^{53}Mn/^{55}Mn$ ratio measured in bulk chondrites (Shukolyukov and Lugmair 2006) and to the LEW 86010 plutonic angrite (Amelin 2008), without taking into account an RSF measured on carbonate minerals. To consistently compare these ages with the Sutter's Mill data, we have reanchored their data to the U-corrected Pb-Pb ages of D'Orbigny and compared them with the Pb-Pb ages of CAIs (Brennecka and Wadhwa 2012; Connelly et al. 2012). The ages from De Leuw et al. (2009) are between approximately 1.5 and 2.7 Myr after CAI formation, and an RSF correction would make the ages even younger. These ages are old compared with previously reported carbonate Mn-Cr ages of approximately 20 Myr in CI chondrites (Endress et al. 1996). Yet again, the young CI ages were anchored to Mn-Cr ages of CAIs from Birck and Allègre (1988), which have since been revised to lower values (Trinquier et al. 2008). When reanchored to D'Orbigny, the age of CI carbonates measured by Endress et al. (1996) corresponds to approximately 6.4 Myr after CAI formation. Their measurements, however, did not include carbonate RSF analyses, and therefore the correction factor to the isochron is unknown.

Our results on SM51-1 show that aqueous alteration was occurring on the CM parent body by 2.4 to 5.0 Myr after CAI formation, consistent with the late accretion model of carbonaceous chondrites forming after differentiated parent bodies (Kleine et al. 2005). Hf-W ages of angrites and iron meteorites indicate that core formation in these bodies occurred no later than 2 Myr after CAI formation. Furthermore, thermodynamic modeling of planetesimals heated by ^{26}Al reveals that there is a time gap between accretion and core formation, suggesting that differentiated meteorites accreted approximately 1.5 Myr after CAI formation (Qin et al. 2008; Kleine et al. 2012). Pb-Pb and Al-Mg dating of chondrules from a variety of chondrites (including CV, CR, CO, and UOCs) shows that most chondrules were formed within approximately 2–3 Myr of CAI formation (Kita and Ushikubo 2012), after the suggested timing of core formation in differentiated bodies. Al-Mg ages of some chondrules in CR chondrites are shown to have formation ages >3 Myr (Nagashima et al. 2008). However, the Al-Mg system is currently under examination as to whether it has been disturbed from aqueous alteration or other parent body processes (Alexander and Ebel 2012; Kita and Ushikubo 2012). Chondrules in CM chondrites have not been dated due to their heavily altered nature; therefore, other classes can be used as a proxy. If accurate, the chondrule formation time scale would allow for a span of 1–2 Myr for parent body accretion and the early onset of alteration; however, this would require aqueous alteration to occur nearly immediately after the accretion of the CM parent body. Secondary alteration would begin once temperatures became high enough to melt the accreted ice on the chondrite parent body, either occurring from internal heating due to the decay of radionuclides such as ^{26}Al, or from other late-stage processes, such as impact heating. Models of internal parent body heating from ^{26}Al by Fujiya et al. (2012, 2013) confirm that optimum carbonate-forming temperatures would easily be reached within 1–2 Myr, depending on the accretion time and radius of the CM parent body. Similar studies in CO and CV chondrites support the early accretion and aqueous alteration of carbonaceous chondrites (Doyle et al. 2013; Krot et al. 2013).

Relative Ages of Dolomite and Calcite

Although the calcite and dolomite crystals in SM51-1 are intergrown (see Fig. 1a), they did not likely form in equilibrium from the same fluid (Riciputi et al. 1994). Petrographic observations show instances of dolomite encompassing calcite (Fig. 1b), suggesting a later formation of dolomite. Furthermore, calcite formation temperatures in CM chondrites as estimated by clumped isotope thermometry (Guo and Eiler 2007) and O-isotope fractionation (Clayton and Mayeda 1984) suggest formation at temperatures of 0–30 °C. Dolomites in CM chondrites have been estimated to form at higher temperatures of approximately 120 °C, using an O-isotope dolomite-serpentine geothermometer (Nakamura et al. 2003). In the hypothesis of parent body alteration due to the heating from ^{26}Al decay, the carbonate phases can be interpreted as calcite precipitating first, with dolomites forming afterward under higher temperature conditions and progressive alteration (Rubin et al. 2007; Fujiya et al. 2012). However, Lee et al. (2012) have interpreted similar carbonate textures from the CM 2.1 chondrite QUE 93005 as forming in the reverse order, where breunnerite ($[Mg,Fe]CO_3$) crystallizes first on pore

margins, followed by dolomite, then calcite filling in as pore center.

O-isotopes in calcite and dolomite grains in Sutter's Mill SM51-1 were measured and reported in Jenniskens et al. (2012). The calcite grains appear to track fluid evolution, as the O-isotopes plot on an array with a slope nearly identical to calcites in other CM chondrites (Benedix et al. 2003). In contrast, dolomite grains from SM51-1 plot in a tightly clustered region near the lower $\Delta^{17}O$ end of the calcite array, indicating stringent physicochemical conditions upon formation (Jenniskens et al. 2012). If formed from the same fluid, dolomite formation may have occurred between (or simultaneous with) calcite precipitation events; otherwise, dolomite may have formed under distinct temperature and fluid chemistry altogether. Unfortunately, we were not able to locate any calcite crystals with Mn and Cr count rates high enough to use for radiometric dating to verify a relative formation time scale. Further analysis of calcites in SM51-1 could be of interest to see if one can distinguish the relative Mn-Cr ages of calcites and dolomites. However, considering the current level of uncertainty associated with the Mn-Cr chronometer, resolving the alteration ages between dolomite and calcite would require that the minerals precipitated in distinct events at least hundreds of thousands of years apart.

Relevance to Other Measured Isotopic Systems in Sutter's Mill

Recent studies of the Sutter's Mill piece SM51 have suggested the disturbance of some isotopic systems. Walker et al. (2013) reported on ^{187}Re-^{187}Os systematics measured from whole-rock powders taken from fresh interior portions of the meteorite. Their results show evidence for a late-stage disturbance to the highly siderophile elements (HSE), within the last approximately 1 Ga. However, our tight isochron shows that the Mn-Cr systematics were not affected by the HSE mobility that caused the Re-Os system to be disturbed. Our early carbonate-formation age of approximately 4564 Ma is contemporaneous with that of other CM chondrites (Fujiya et al. 2012), and can be reconciled if the dolomite was not the mineralogic carrier of the disturbances to the Re-Os system. Both rhenium and osmium are highly siderophile, and are probably sequestered in iron-rich secondary phases, rather than in the iron-poor carbonates measured here. Redistribution of the rhenium and osmium isotopes can occur on a scale of millimeters to centimeters in a sample, and may be due to aqueous alteration or shock on the parent body, or to later terrestrial weathering (Walker et al. 2002). Such a late-stage disturbance suggests that the cause was probably terrestrial weathering or shock. A rainfall event was documented before the finding of SM51 (Jenniskens et al. 2012), and could have been sufficient to mobilize highly siderophile elements (Walker et al. 2013). Although no terrestrial weathering veins are seen in the section SM51-1 studied here, iron-bearing minerals are generally the most readily oxidized by the Earth's atmosphere (Bland et al. 2006). Minor terrestrial weathering due to the rainfall event could plausibly disturb the HSE elements, without affecting the iron-free dolomite grains, supporting the validity of our isochron.

The Mn-Cr system has been studied in SM51 in other capacities. Bulk Mn-Cr systematics from powders were investigated by Jenniskens et al. (2012). The isotopic data plot on a linear correlation with other carbonaceous chondrites, with a $^{53}Mn/^{55}Mn$ ratio of $(5.90 \pm 0.67) \times 10^{-6}$—a higher ratio than we obtain from Sutter's Mill dolomite ($3.42 \pm 0.86 \times 10^{-6}$). Although many questions remain regarding the meaning of this bulk Mn-Cr carbonaceous chondrite array, it has been suggested that the bulk trend represents a large-scale fractionation of Mn and Cr in the early solar nebula, with the possibility of disturbance during planetesimal formation in the nebula (e.g., Shukolyukov and Lugmair 2006; Scott and Sanders 2009; Jenniskens et al. 2012). Regardless of the interpretation of the bulk isochron, Sutter's Mill dolomites record a younger age than the bulk trend, consistent with a later stage Mn redistribution occurring on the CM parent body. Mn-Cr isotopes have also been measured in mineral leachates from SM51 (Yamakawa and Yin 2013). The leaching was performed to identify the mineral phases containing distinct manganese and Cr isotopic signatures (Yamakawa and Yin 2013). Leachate L1 in their study is comprised of easily soluble minerals that are dissolved by weak acids, including carbonates and sulfides. L1 carries a large excess of ^{53}Cr compared with the other leachates, indicating that ^{53}Mn was alive at the time of formation of the L1 minerals. The L1 leachate plots below the bulk Mn-Cr isochron, suggesting that the leachate minerals were formed during a secondary process, such as aqueous alteration occurring postaccretion of the parent body of Sutter's Mill. Their carbonate leachate result is consistent with this study in that it demonstrates that ^{53}Mn was alive at the time of aqueous alteration on the Sutter's Mill parent body.

CONCLUSIONS

The results of our investigation of Sutter's Mill SM51-1 are consistent with the CM 2.0/2.1 classification. The Mn-Cr radiometric dating of

secondary dolomites from SM51-1 reveals ages contemporaneous with dolomite grains in other CM chondrites. In addition, the ages of dolomite in CI chondrites and Tagish Lake are also contemporaneous, suggesting that parallel aqueous alteration events occurred on the various parent bodies. We stress that interlaboratory comparisons of Mn-Cr measurements in carbonates of carbonaceous chondrites are possible only if each measurement has been acquired self-consistently using the same standards to correct for RSF. We have used the same standard with similar relative sensitivity factors as used in Fujiya et al. (2012, 2013), and make comparisons to their data set. Our SM51-1 dolomite age of 4563.7 $^{+1.1}/_{-1.5}$ Ma suggests that aqueous alteration occurred early in the parent body history, probably due to heating from ^{26}Al decay. There is no observable correlation between the petrologic type for CM chondrites and the age of alteration, and any distinct carbonate forming events are currently unresolved. The well-defined isochron presented here suggests that any subsequent processing to SM51, whether thermal, impact, or terrestrial, did not disturb the Mn-Cr system in secondary dolomites.

Acknowledgments—This research is supported by NASA through NASA grant NNX11AG78G (G. R. Huss, PI), NAI cooperative agreement NNA04CC08A (K. Meech, PI), and NNX11AJ51G (Q. Z. Yin, PI). The authors would like to thank C. Alexander, W. Fujiya, and Y. Guan for their reviews, which helped to significantly improve this manuscript. This is Hawaii Institute of Geophysics and Planetology publication #2029, and School of Ocean and Earth Science and Technology publication #9089.

Editorial Handling—Dr. Gretchen Benedix

REFERENCES

Alexander C. M. O'D. and Ebel D. S. 2012. Questions, questions: Can the contradictions between the petrologic, isotopic, thermodynamic, and astrophysical constraints on chondrule formation be resolved? *Meteoritics & Planetary Science* 47:1157–1175.

Amelin Y. 2008. U-Pb ages of angrites. *Geochimica et Cosmochimica Acta* 72:221–232.

Amelin Y., Kaltenbach A., Iizuka T., Stirling C. H., Ireland T. R., Petaev M., and Jacobsen S. B. 2010. U-Pb chronology of the solar system's oldest solids with variable ^{238}U/^{235}U. *Earth and Planetary Science Letters* 300:343–350.

Baum E. M., Knox H. D., and Miller R. T. 2002. *Nuclides and isotopes*, 16th ed. Niskayuna, New York: Knolls Atomic Power Laboratory, Inc. 47 p.

Benedix G. K., Leshin L. A., Farquhar J., Jackson T., and Thiemens M. H. 2003. Carbonates in CM2 chondrites: Constraints on alteration conditions from oxygen isotopic compositions and petrographic observations. *Geochimica et Cosmochimica Acta* 67:1577–1588.

Birck J.-L. and Allègre C. J. 1988. Manganese-chromium isotope systematics and the development of the early solar system. *Nature* 331:579–584.

Bland P. A., Zolensky M. E., Benedix G. K., and Sephton M. A. 2006. Weathering of chondritic meteorites. In *Meteorites and the early solar system* II, edited by Lauretta D. S. and McSween H. Y. Jr. Tucson, Arizona: University of Arizona Press. pp.853–867.

Brennecka G. A. and Wadhwa M. 2012. Uranium isotope compositions of the basaltic angrite meteorites and the chronological implications for the early solar system. *Proceedings of the National Academy of Sciences* 109:9299–9303.

Clayton R. N. and Mayeda T. K. 1984. The oxygen isotope record in Murchison and other carbonaceous chondrites. *Earth and Planetary Science Letters* 67:151–161.

Connelly J. N., Bizzarro M., Krot A. N., Nordlund Å., Wielandt D., and Ivanova M. A. 2012. The absolute chronology and thermal processing of solids in the solar protoplanetary disk. *Science* 338:651–655.

De Leuw S., Rubin A. E., Schmitt A. K., and Wasson J. T. 2009. ^{53}Mn-^{53}Cr systematics of carbonates in CM chondrites: Implications for the timing and duration of aqueous alteration. *Geochimica et Cosmochimica Acta* 73:7433–7442.

De Leuw S., Rubin A. E., and Wasson J. T. 2010. Carbonates in CM chondrites: Complex formational histories and comparison to carbonates in CI chondrites. *Meteoritics and Planetary Science* 45:513–530.

Doyle P. M., Krot A. N., and Nagashima K. 2013. Oxygen-isotopes of fayalite, magnetite and chondrule olivine in the CO (Y-81020, EET 90043) and CO-like (MAC 88107) chondrites. 76th Annual Meteoritical Society Meeting (abstract #5135). *Meteoritics & Planetary Science* 48.

Endress M., Zinner E., and Bischoff A. 1996. Early aqueous activity on primitive meteorite parent bodies. *Nature* 379:701–703.

Fujiya W., Sugiura N., Hotta H., Ichimura K., and Sano Y. 2012. Evidence for the late formation of hydrous asteroids from young meteoritic carbonates. *Nature Communications* 3:627.

Fujiya W., Sugiura N., Sano Y., and Hiyagon H. 2013. Mn-Cr ages of dolomites in CI chondrites and the Tagish Lake ungrouped carbonaceous chondrite. *Earth and Planetary Science Letters* 362:130–142.

Garvie L. A. J. 2013. Mineralogy of the Sutter's Mill carbonaceous chondrite (abstract #2148). 44th Lunar and Planetary Science Conference. CD-ROM.

Glavin D. P., Kubny A., Jagoutz E., and Lugmair G. W. 2004. Mn-Cr isotope systematics of the D'Orbigny angrite. *Meteoritics & Planetary Science* 39:693–700.

Grady M. M., Fernandes C. D., Gilmour I., Harker A., Preston L., and Verchobsky A. B. 2013. Light element geochemistry and spectroscopy of the Sutter's Mill carbonaceous chondrite (abstract #3000). 44th Lunar and Planetary Science Conference. CD-ROM.

Guo W. and Eiler J. M. 2007. Temperatures of aqueous alteration and evidence for methane generation on the parent bodies of the CM chondrites. *Geochimica et Cosmochimica Acta* 71:5565–5575.

Hoppe P., MacDougall D., and Lugmair G. W. 2007. High spatial resolution ion microprobe measurements refine

chronology of carbonate formation in Orgueil. *Meteoritics & Planetary Science* 42:1309–1320.

Jenniskens P., Fries M. D., Yin Q.-Z., Zolensky M., Krot A. N., Sandford S. A., Sears D., Beauford R., Ebel D. S., Friedrich J. M., Nagashima K., Wimpenny J., Yamakawa A., Nishiizumi K., Hamajima Y., Caffee M. W., Welten K. C., Laubenstein M., Davis A. M., Simon S. B., Heck P. R., Young E. D., Kohl I. E., Thiemens M. H., Nunn M. H., Mikouchi T., Hagiya K., Ohsumi K., Cahill T. A., Lawton J. A., Barnes D., Steele A., Rochette P., Verosub K. L., Gattacceca J., Cooper G., Glavin D. P., Burton A. S., Dworkin J. P., Elsila J. E., Pizzarello S., Ogliore R., Schmitt-Kopplin P., Harir M., Hertkorn N., Verchovsky A., Grady M., Nagao K., Okazaki R., Takechi H., Hiroi T., Smith K., Silber E. A., Brown P. B., Albers J., Klotz D., Hankey M., Matson R., Fries J. A., Puchtel I., Lee C.-T. A., Erdman M. E., Eppich G. R., Roeske S., Gabelica Z., Lerche M., Nuevo M., Girten B., and Worden S. P. 2012. Radar-enabled recover of the Sutter's Mill meteorite, a carbonaceous chondrite regolith breccia. *Science* 338:1583–1587.

Keil K. 2012. Angrites, a small but diverse suite of ancient, silica-undersaturated volcanic-plutonic mafic meteorites, and the history of their parent asteroid. *Chemie der Erde* 72:191–218.

Kita N. T. and Ushikubo T. 2012. Evolution of protoplanetary disk inferred from ^{26}Al chronology of individual chondrules. *Meteoritics & Planetary Science* 47:1108–1119.

Kleine T., Mezger K., Palme H., Scherer E., and Münker C. 2005. Early core formation in asteroids and late accretion of chondrite parent bodies: Evidence from ^{182}Hf-^{182}W in CAIs, metal-rich chondrites, and iron meteorites. *Geochimica et Cosmochimica Acta* 69:5805–5818.

Kleine T., Hans U., Irving A. J., and Bourdon B. 2012. Chronology of the angrite parent body and implications for core formation in protoplanets. *Geochimica et Cosmochimica Acta* 84:186–203.

Krot A. N., Hutcheon I. D., Brearley A. J., Pravdivtseva O. V., Petaev M. I., and Hohenberg C. M. 2006. Timescales and settings for alteration of chondritic meteorites. In *Meteorites and the early solar system* II, edited by Lauretta D. S. and McSween H. Y. Jr. Tucson, Arizona: University of Arizona Press. pp. 525–553.

Krot A. N., Doyle P. M., Nagashima K., Jogo K., Wakita S., Ciesla F. J., and Hutcheon I. D. 2013. Origin of asteroidal water: Constraints from isotopic compositions of aqueously formed minerals. 76th Annual Meteoritical Society Meeting #5161 (abstract).

Lee M. R., Lindgren P., Sofe M. R., Alexander C. M. O'D., and Wang J. 2012. Extended chronologies of aqueous alteration in the CM2 carbonaceous chondrites: Evidence from carbonates in Queen Alexandra Range 93005. *Geochimica et Cosmochimica Acta* 92:148–169.

Lugmair G. W. and Shukolyukov A. 1998. Early solar system timescales according to ^{53}Mn–^{53}Cr systematics. *Geochimica et Cosmochimica Acta* 62:2863–2886.

McKibbin S. J., Ireland T. R., Amelin Y., O'Neill H. S. C., and Holden P. 2013. Mn–Cr relative sensitivity factors for secondary ion mass spectrometry analysis of Mg–Fe–Ca olivine and implications for the Mn–Cr chronology of meteorites. *Geochimica et Cosmochimica Acta* 110:216–228.

Mittlefehldt D. W., Killgore M., and Lee M. T. 2002. Petrology and geochemistry of D'Orbigny, geochemistry of Sahara 99555, and the origin of angrites. *Meteoritics and Planetary Science* 37:345–369.

Nagashima K., Krot A. N., and Huss G. R. 2008. ^{26}Al in chondrules from CR carbonaceous chondrites (abstract #2224). 39th Lunar and Planetary Science Conference. CD-ROM.

Nakamura T., Noguchi T., and Yoneda S. 2003. The conditions of aqueous alteration reaction recorded in the Sayama CM2 chondrite (abstract #5080). *Meteoritics & Planetary Science* 38:A47.

Ogliore R. C., Huss G. R., and Nagashima N. 2011. Ratio estimation in SIMS analysis. *Nuclear Instruments and Methods in Physics Research B* 269:1910–1918.

Papanastassiou D. A. 1986. Chromium isotopic anomalies in the Allende meteorite. *The Astrophysical Journal* 308:L27–L30.

Petitat M., McKeegan K., Gounelle M., Mostefaoui S., Marrocchi Y., Meibom A., and Leshin L. A. 2009. Duration and sequence of carbonate crystallization on the Orgueil protolith: ^{53}Mn-^{53}Cr systematics of their evolution in O and C isotopic evolution (abstract #1288). 40th Lunar and Planetary Science Conference. CD-ROM.

Petitat M., Marrocchi Y., McKeegan K. D., Mostefaoui S., Meibom A., Zolensky M. E., and Gounelle M. 2011. ^{53}Mn-^{53}Cr ages of Kaidun carbonates. *Meteoritics & Planetary Science* 46:275–283.

Pingitore N. E., Eastman M. P., Sandidge M., Oden K., and Freiha B. 1988. The coprecipitation of manganese (II) with calcite: An experimental study. *Marine Chemistry* 25:107–120.

Qin L., Dauphas N., Wadhwa M., Masarik J., and Janney P. E. 2008. Rapid accretion and differentiation of iron meteorite parent bodies inferred from ^{182}Hf-^{182}W chronometry and thermal modeling. *Earth and Planetary Science Letters* 273:94–104.

Riciputi L. R., McSween H. Y., Johnson C. A., and Prinz M. 1994. Minor and trace element concentrations in carbonates of carbonaceous chondrites, and implications for the compositions of coexisting fluids. *Geochimica et Cosmochimica Acta* 58:1343–1351.

Rubin A. E., Trigo-Rodríguez J. M., Huber H., and Wasson J. T. 2007. Progressive alteration of CM carbonaceous chondrites. *Geochimica et Cosmochimica Acta* 71:2361–2382.

Scott E. R. D. and Sanders I. S. 2009. Implications of the carbonaceous chondrite Mn-Cr isochron for the formation of early refractory planetesimals and chondrules. *Geochimica et Cosmochimica Acta* 73:5137–5149.

Shukolyukov A. and Lugmair G. 2006. Manganese–chromium isotope systematics of carbonaceous chondrites. *Earth and Planetary Science Letters* 250:200–213.

Sugiura N., Ichimura K., Fujiya W., and Takahata N. 2010. Mn/Cr relative sensitivity factors for sythetic calcium carbonate measured with a NanoSIMS ion microprobe. *Geochemical Journal* 44:e11–e16.

Trinquier A., Birck J.-L., Allègre C. J., Göpel C., and Ulfbeck D. 2008. ^{53}Mn-^{53}Cr systematics of the early solar system revisited. *Geochimica et Cosmochimica Acta* 72:5146–5163.

Tyra M. A., Brearley A. J., Hutcheon I. D., Ramon E., Matzel J., and Weber P. 2009. Carbonate formation timescales vary between CM1 chondrites ALH 84051 and

ALH 84034 (abstract #2474). 40th Lunar and Planetary Science Conference. CD-ROM.

Walker R. J., Horan M. F., Morgan J. W., Becker H., Grossman J. N., and Rubin A. E. 2002. Comparative ^{187}Re-^{187}Os systematics of chondrites: Implications regarding early solar system processes. *Geochimica et Cosmochimica Acta* 66:4187–4201.

Walker R. J., Puchtel I. S., and Yin Q.-Z. 2013. ^{187}Re-^{187}Os isotopic and highly siderophile element abundance systematics of the Sutter's Mill meteorite: Clues to late-stage secondary processes acting on chondrites (abstract #1964). 44th Lunar and Planetary Science Conference. CD-ROM.

Yamakawa A. and Yin Q.-Z. 2013. The chromium isotopic studies of Sutter's Mill CM-type carbonaceous chondrite: Implications for isotopic heterogeneities of the solar system (abstract #2418). 44th Lunar and Planetary Science Conference. CD-ROM.

Ziegler K. and Garvie A. J. 2013. Bulk oxygen-isotope compositions of different lithologies in Sutter's Mill (abstract #5225). 76th Annual Meteoritical Society Meeting. *Meteoritics & Planetary Science* 48.